Journal of the Serbian Chemical Society
JSCS-info@shd.org.rs • www.shd.org.rs/JSCS
*J. Serb. Chem. Soc. 91* (0) 1–12 (2026)
*JSCS–13775*
*Original scientific paper*
Published 21 Aug 2026

# Process optimization and economic calculation of photocatalytic degradation of methylene blue over sulfur-doped g-$C_3N_4$

WEI LI[1]* and SHUYU CAO[2]

[1]*Department of Economics, Heilongjiang University of Finance and Economics, Harbin 150025, China and* [2]*Department of Science and Technology, Heilongjiang University of Finance and Economics, Harbin 150025, China*

(Received 12 February, revised 10 April, accepted 19 May 2026)

*Abstract*: Sulfur doping has been considered an effective strategy to enhance the photocatalytic activity of graphitic carbon nitride (g-$C_3N_4$). However, there are no reports on the process optimization and economic calculation to determine the optimal photocatalytic parameters and compare the operating costs, respectively. In this work, sulfur-doped g-$C_3N_4$ (S/g-$C_3N_4$) was prepared *in situ* by a one-pot pyrolysis approach using thiourea as the precursor and sulfur source. S/g-$C_3N_4$ was characterized by various instrumental techniques. Response surface methodology (RSM) was employed to determine the optimal photocatalytic conditions for the degradation of Methylene blue (MB) over S/g-$C_3N_4$. A central composite design (CCD) with four factors at five levels was established, comprising 30 experimental runs. The optimal conditions were determined as an initial MB concentration of 27.6 mg $L^{-1}$, a catalyst dosage of 4.1 g $L^{-1}$, a solution pH of 8.7 and a reaction time of 127 min. Under these conditions, the predicted degradation efficiency could reach 99.94 %, while the experimental value was 99.5 %. Cost accounting indicated that the optimization substantially reduced direct costs, greatly improved equipment utilization, and enhanced operational flexibility. This work will lay key foundation for cost control and efficiency improvement in the scale-up application of g-$C_3N_4$-based photocatalysts.

*Keywords*: graphitic carbon nitride; photocatalyst; response surface methodology; cost accounting.

## INTRODUCTION

Resource shortages and environmental pollution are closely related to our quality of life and health conditions, and have drawn considerable attention from governments around the world. Among the two, the issues caused by environmental pollution are more significant.[1] Among various kinds of environmental pollution, organic dye wastewater has attracted the most attention because of its high

* Corresponding author. E-mail: lilidezhicheng@sina.com
https://doi.org/10.2298/JSC260212027L

concentration, diverse composition, difficult decolorization, widespread pollution and complex structure. At present, there are many technologies to treat organic dye wastewater, including adsorption, membrane separation, biodegradeation, extraction, oxidation and so on.[2] In recent years, the development of advanced oxidation technologies represented by photocatalytic oxidation has attracted considerable attention. The use of photocatalytic materials to purify water has become a high-tech environmental purification technology of global concern.[3]

In recent decades, a variety of novel visible-light-response photocatalytic materials have been developed, such as bismuth oxyhalides, metal-organic frameworks, $ZnIn_2S_4$, $CuFeS_2$, $WO_3$, $CuWO_4$, $Cu_2SnS_3$ and others. These materials have high visible-light catalytic stability and activity.[4–7] However, the precious metals in the components increase the preparation and production costs of photocatalytic materials. At the same time, they have certain toxicity and the potential to pollute the water environment. Therefore, these materials are not suitable for large-scale practical applications. Graphitic carbon nitride (g-$C_3N_4$) is a new type of non-metallic semiconductor with a band gap of about 2.7 eV, which can achieve visible light response and make full use of solar energy. Moreover, g-$C_3N_4$ has a stable structure, controllable performance, a non-toxic and harmless nature, acid and alkali resistance, and light corrosion resistance. It has become a hotspot in the research field of photocatalytic materials.[8,9] However, the shortcomings of g-$C_3N_4$, such as fast electron-hole recombination and a small specific surface area, limit its practical application. Therefore, heterojunction construction, doping modification, microstructure regulation and other methods have been employed to improve the photocatalytic activity of g-$C_3N_4$.[10,11] Among them, doping with non-metallic elements could effectively change the electronic band structure of g-$C_3N_4$, thereby improving its photocatalytic activity.[12] Xu and coworkers successfully prepared g-$C_3N_4$ with nitrogen defects and sulfur doping *via* a cold plasma technique. S--doping could offer more active sites for the photocatalytic process and enhance the stability of N defects. The visible light photocatalytic activity of S-doped g--$C_3N_4$ was 11.25 times higher than that of pure g-$C_3N_4$.[13] Ma *et al.* used the dielectric barrier discharge (DBD) plasma to obtain an S-doped g-$C_3N_4$ photocatalyst under an $H_2S$ atmosphere. They found that DBD plasma treatment could make more sulfur be doped into the g-$C_3N_4$ lattice than traditional roasting approach. The as-prepared S-doped g-$C_3N_4$ exhibited much higher photocatalytic degradation efficiency of rhodamine B (RhB).[14] In addition, a porous S-doped g-$C_3N_4$ was successfully prepared *via* one-step calcination method by Yang and coworkers. The as-prepared porous S-doped g-$C_3N_4$ displayed approximately 6.2 times higher peroxymonosulfate activation capacity for the degradation of RhB than pristine g-$C_3N_4$ under visible light irradiation.[15] Song *et al*. employed urea and thiourea as precursors to prepare S-doped g-$C_3N_4$ nanosheets through physical steam activation. The as-prepared photocatalyst exhibited 2.1 and 5.52 fold higher

decomposition efficiency and reaction rate for the photodegradation of Methylene blue (MB) dye than bulk g-$C_3N_4$, respectively.[16] Overall, S doping has been proven to be an efficient strategy to improve light absorption and photogenerated electron–hole separation, consequently boosting the photocatalytic activity of g-$C_3N_4$.[17] However, there are few reports on the process optimization of photocatalytic degradation of organic pollutants over S-doped g-$C_3N_4$. Response surface methodology (RSM) based on a central composite design (CCD) is a widely used process parameter optimization method.[18–20] This methodology includes experimental condition design and parameter optimization. The specific steps of this methodology can be divided into the following four aspects:[21,22] 1) determination of the variables and experimental design, 2) evaluation of the parameters for mathematical model regression analysis, 3) prediction of the model response and 4) confirmation of the accuracy of the model. In addition, as far as we know, the economic calculation of photocatalytic degradation of organic pollutants over S-doped g-$C_3N_4$ before and after process optimization has not been investigated.

Therefore, in this work, S-doped g-$C_3N_4$ was prepared by a facile one-pot pyrolysis approach using thiourea as the precursor and sulfur source to realize *in situ* S doping and achieve high photocatalytic activity. Based on the characterization analyses and photocatalytic performance evaluation of S-doped g-$C_3N_4$, the RSM method was employed for the first time to optimize the process of MB photodegradation over S-doped g-$C_3N_4$ to determine the optimal operating parameters. Moreover, the economic calculations before and after optimization were performed for the first time. Therefore, this work will lay an engineering and cost foundation for the large-scale practical applications of g-$C_3N_4$-based photocatalysts.

## EXPERIMENTAL

### *Preparation of S-doped g-$C_3N_4$*

A facile one-pot pyrolysis approach was employed to prepare in situ S-doped g-$C_3N_4$ using thiourea as the precursor and sulfur source.[23] The specific procedures are as follows: 15 g of thiourea was weighed and put into a 100 mL crucible, and then heated from room temperature to 550 °C at a heating rate of 20 °C/min in a muffle furnace. After being kept for 4 h, the sample was cooled to room temperature in the furnace. Finally, it was ground into powder for subsequent use.

### *Characterization techniques*

X-ray diffraction (XRD), Fourier transform infrared spectroscopy (FTIR), field emission scanning electron microscopy (FESEM), transmission electron microscopy (TEM) and UV–Vis diffuse reflectance spectroscopy (UV–Vis DRS) were used to characterize the as-prepared samples. The detailed information is provided in the supplementary file.

### *Photocatalytic experiments*

The photocatalytic performance of S-doped g-$C_3N_4$ was evaluated using MB dye as the target pollutant. The experimental procedure is provided in the Supplementary material to this paper.

*RSM optimization method*

In this work, four parameters were selected as variables, namely the initial MB concentration (mg $L^{-1}$), catalyst dosage (g $L^{-1}$), solution pH and reaction time (min), which were labeled as $X_1$, $X_2$, $X_3$ and $X_4$, respectively. At the same time, the degradation rate of MB dye was used as the output response ($Y$). The detailed descriptions of experimental design, mathematical modeling and response optimization are provided in the Supplementary material. In addition, the range and the level of independent variables are shown in Table S-I of the Supplementary material.

*Economic calculation method*

Generally, the standardized economic calculation for a wastewater treatment process included three main parts: raw material cost, operation cost and integrated cost.[24-26] Their calculation methods are provided in the Supplementary material.

## RESULTS AND DISCUSSION

### *Characterization of S-doped g-$C_3N_4$*

Fig. 1A presents the XRD pattern of the S-doped g-$C_3N_4$ sample. The XRD pattern shows two prominent diffraction peaks located at 2$\theta$ 13 and 27.5°. The peak at 13° belongs to the in-plane ordering of triazine units and is indexed to the (100) crystal plane of g-$C_3N_4$, whereas the peak at 27.5° corresponds to the interlayer stacking of aromatic layers and is assigned to the (002) crystal plane of g-$C_3N_4$.[27] The FT-IR spectrum of S-doped g-$C_3N_4$ is displayed in Fig. 1B. The absorption bands in the 1225–1640 $cm^{-1}$ region are assigned to stretching vibrations of C–N and C=N bonds within the N-containing ring framework, together with exocyclic C–N stretching.[28] The broad band at 3135 $cm^{-1}$ is associated with N–H stretching vibrations,[29] while the band at 796 $cm^{-1}$ is attributed to the bending vibration of the C–N ring.[30]

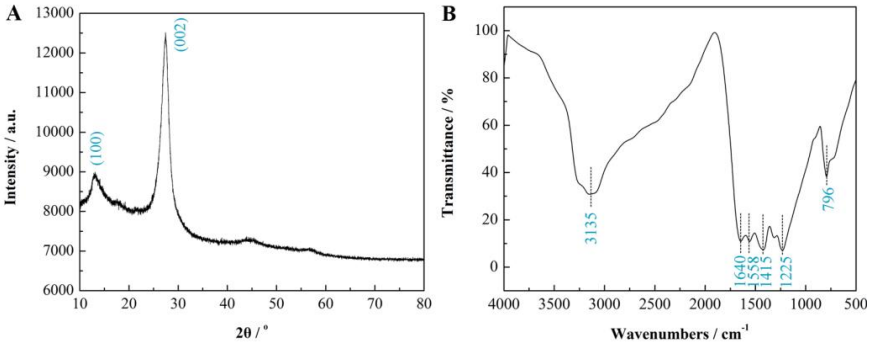


Fig. 1. A) XRD pattern and B) FTIR spectrum of S-doped g-$C_3N_4$.

Fig. 2A gives an FESEM image of S-doped g-$C_3N_4$, displaying a non-uniform particulate morphology in which the particles are irregularly agglomerated, consistent with the typical morphology of g-$C_3N_4$.[31] Fig. 2B shows a TEM image of the

S-doped g-$C_3N_4$ sample. It can be seen that the as-prepared sample has a typical thin-layer structure with some wrinkles, similar to graphene. This thin-layer structure will further increase the specific surface area of the S-doped g-$C_3N_4$ sample, thereby improving the adsorption capacity and photocatalytic activity of the sample.[32] From the energy-dispersive spectrum (EDS) of S-doped g-$C_3N_4$ (Fig. 2C), it can be clearly seen that the as-prepared sample contains three main elements C, N and S, which indicates that S has been successfully introduced into g-$C_3N_4$. In addition, no characteristic diffraction peak or absorption peak belonging to S was found in the XRD pattern and the FTIR spectrum, which implies that S might enter the crystal structure of g-$C_3N_4$ and replace C or N, rather than as impurities.[13–16]

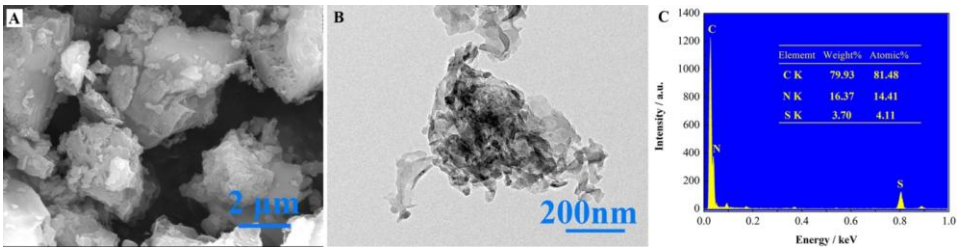


Fig. 2. A) FESEM, B) TEM and C) EDS images of S-doped g-$C_3N_4$.

Fig. 3A shows the UV–Vis DRS spectrum of S-doped g-$C_3N_4$, from which it can be observed that the S-doped g-$C_3N_4$ sample has strong visible-light absorption and an absorption edge is located at approximately 412 nm. According to the extrapolation of $(F(R)–h\nu)^{1/2}$ curve *vs.* photon energy $h\nu$ (Fig. 3B), the band gap ($E_g$) of S-doped g-$C_3N_4$ is estimated to be 2.63 eV, in agreement with literature reports.[33] Notably, the as-prepared sample exhibits an additional absorption feature near 645 nm in the UV–Vis DRS spectrum, corresponding to an $E_g$ of 1.81 eV. This might be associated with an S-induced impurity energy level in the band structure,[34] which can facilitate the enhancement of photocatalytic performance.

*Process optimization of MB photodegradation over S-doped g-$C_3N_4$*

To evaluate the photocatalytic performance of S-doped g-$C_3N_4$, MB with analytical purity was used as the target pollutant under the conditions of 10 mg $L^{-1}$ MB, 5.0 g $L^{-1}$ S-doped g-$C_3N_4$, pH 7 and room temperature. As shown in Fig. 4A, after 60 min in the dark to reach adsorption equilibrium, the removal rate of MB is only 9.4 %, suggesting that the contribution of adsorption to MB removal can be neglected. However, after 120 min of photocatalytic irradiation, the corresponding degradation rate increased to 95.8 %. Accordingly, the as-prepared S-doped g-$C_3N_4$ sample exhibits stronger photocatalytic performance toward MB degradation. Additionally, this photocatalytic process follows the pseudo-first-order kinetic model (Fig. 4B), with a reaction rate constant of 0.02296 $min^{-1}$. The UV–Vis absorption spectra of the MB solution during different photocatalytic periods are

presented in Fig. 4C, where it can be seen that the main absorption peak of the MB dye molecule at 650 nm disappeared after 120 min of photocatalytic reaction, indicating that the dye molecule has been decomposed. In addition, the removal percentage of total organic carbon (TOC) after 120 min of photocatalytic irradiation was measured as 78.4 %. Therefore, it can be supposed that the MB dye was decomposed into $CO_2$, $H_2O$, and other low-molecular-weight substances.

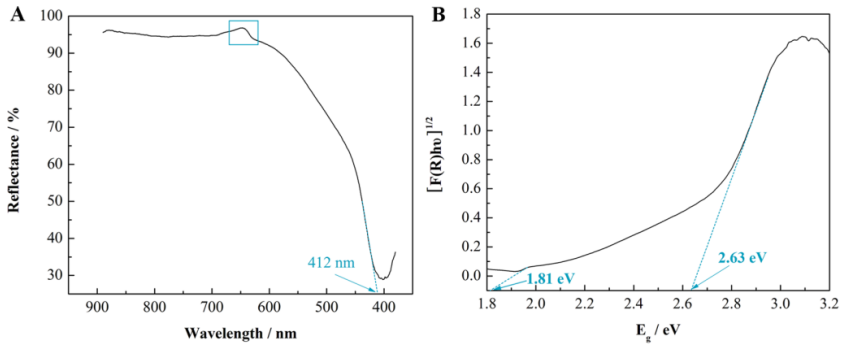


Fig. 3. A) UV–Vis DRS spectrum and B) $(F(R)–h\nu)^{1/2}$ *versus* $h\nu$ curve of S-doped g-$C_3N_4$.

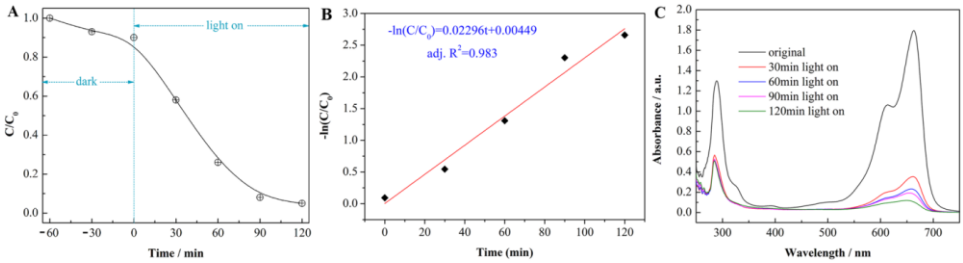


Fig. 4. A) Photocatalytic performance toward MB degradation over S-doped g-$C_3N_4$; B) fitting line of the pseudo-first-order kinetic model; C) UV–Vis absorption spectra of the MB solution during different photocatalytic periods.

Based on the above results, the effects of different experimental parameters on the degradation rate of MB dye were evaluated by RSM. According to the CCD, an experimental scheme with 4 factors and 5 levels was designed, and a total of 30 sets of experiments were carried out. The CCD experimental matrix is listed in Table S-II of the Supplementary material, along with the experimental and predicted values of the response *Y*. Among them, six groups of experiments are replicate experiments at the center point, which ensures that the relative error of the experiment is small. Their close response values mean higher experimental accuracy.[35]

To predict the response value, the experimental values were fitted by a second--order polynomial regression model, and the results are shown as:

$$Y = 66.46 + 5.82X_1 - 13.35X_2 + 7.62X_3 + 12.70X_4 - 2.74X_1X_2 + \\ + 1.69X_1X_3 + 1.70X_1X_4 + 0.79X_2X_3 + 0.21X_2X_4 - 1.17X_3X_4 - \\ - 2.48X_1^2 - 3.90X_2^2 - 10.22X_3^2 - 2.61X_4^2 \quad (1)$$

From the analysis of variance (ANOVA, Table S-III of the Supplementary material), it can be seen that the $F$ value is 8.09, which is much higher than the standard value $F_{0.05} = 2.42$, which means that the second-order polynomial model is highly significant. In addition, as listed in Table S-II, the experimental and predicted values of the response $Y$ are relatively close, with a correlation coefficient of $R^2 = 0.9588$. This is the main criterion for evaluating the correlation between the experimental and predicted values.[36]

Moreover, the predicted response values are in good agreement with the experimental values (Fig. S-2 of the Supplementary material). Furthermore, the *Prob* > $F$ value is less than 0.0500, which means that the influence of the variable is significant, whereas the value greater than 0.1000, indicates that the influence of the variable is not significant.[37] Therefore, in this work, it can be seen from Table S-III that $X_1$, $X_2$, $X_3$, $X_4$, $X_1X_3$, $X_1X_4$, $X_1^2$, $X_3^2$ and $X_4^2$ are the significant influencing variables during the MB photodegradation over S-doped g-$C_3N_4$. In addition, the statistical analysis of the experimental data indicates that the initial MB dye concentration, S-doped g-$C_3N_4$ dosage, solution pH and reaction time have significant effects on MB photodegradation.

The three-dimensional (3D) response surface plots of the interaction effect between two factors are shown in Fig. 5, including the interactions between initial MB concentration and S-doped g-$C_3N_4$ dosage, initial MB concentration and solution pH, initial MB concentration and reaction time, S-doped g-$C_3N_4$ dosage and solution pH, S-doped g-$C_3N_4$ dosage and reaction time and solution pH and reaction time. It can be seen that the degradation rate of MB increases with the decrease in the initial MB concentration and the increase in the S-doped g-$C_3N_4$ dosage (Fig. 5A); increases with the decrease in the initial MB concentration and the increase in the solution pH (Fig. 5B); increases with the decrease in the initial MB concentration and the increase of the reaction time (Fig. 5C); increases with the increase of the S-doped g-$C_3N_4$ dosage and the solution pH (Fig. 5D); increases with the increase in the S-doped g-$C_3N_4$ dosage and the reaction time (Fig. 5E); increases with the increase in the reaction time and the solution pH (Fig. 5F). According to the prediction model, the process parameters of MB photodegradation over the S-doped g-$C_3N_4$ photocatalyst are optimized as follows: the initial MB concentration is 27.6 mg $L^{-1}$, the S-doped g-$C_3N_4$ dosage is 4.1 g $L^{-1}$, the solution pH is 8.7, and the reaction time is 127 min. Under these optimal conditions, the predicted degradation rate of MB can reach 99.94 %. Under the identical conditions, the experimental value of the MB degradation rate is 99.5 %, showing excellent agreement with the model prediction.

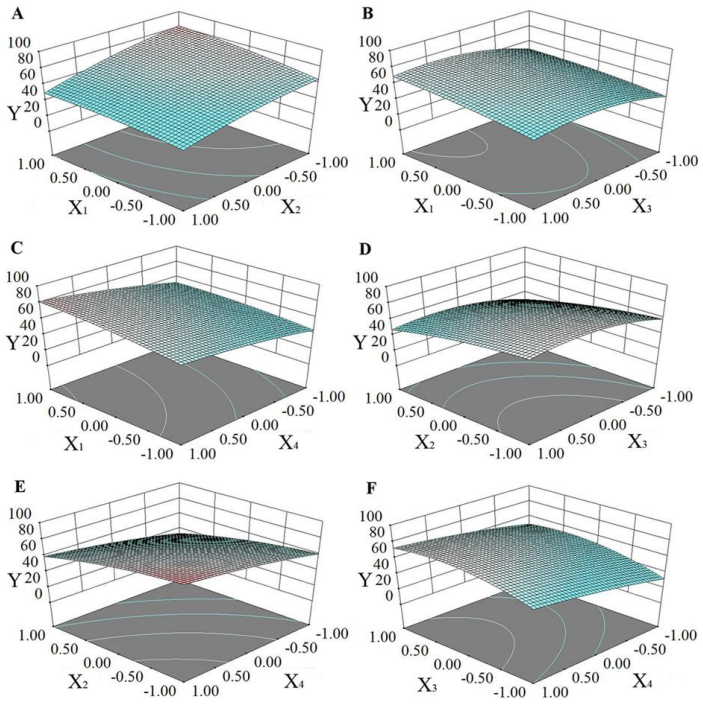


Fig. 5. 3D response surface of MB photodegradation ($Y$) over S-doped g-$C_3N_4$ with the interaction effect between: A) initial MB concentration ($X_1$) and S-doped g-$C_3N_4$ dosage ($X_2$), B) initial MB concentration ($X_1$) and solution pH ($X_3$), C) initial MB concentration ($X_1$) and reaction time ($X_4$), D) S-doped g-$C_3N_4$ dosage ($X_2$) and solution pH ($X_3$), E) S-doped g-$C_3N_4$ dosage ($X_2$) and reaction time ($X_4$) and F) solution pH ($X_3$) and reaction time ($X_4$).

*Economic calculation of MB photodegradation over S-doped g-$C_3N_4$*

*1) Comparative analysis of raw material cost*. Table S-IV of the Supplementary material provides the comparative analysis of raw material cost before and after optimization. Before optimization, the catalyst cost for treating 1 $m^3$ of MB wastewater was 5 kg×80 CNY $kg^{-1}$ = 400 CNY. After optimization, the corresponding cost for treating 1 $m^3$ of MB wastewater was 4.1 kg×80 CNY $kg^{-1}$ = 328 CNY. Therefore, the catalyst cost for treating 1 $m^3$ wastewater was reduced by 72 CNY, with a decrease of 17.8 %. Moreover, after optimization, the pH value of MB solution was adjusted from 7.0 to 8.7, so sodium hydroxide needed to be added to adjust the pH value. Based on the calculation of the acid-base balance, 0.12 kg of sodium hydroxide was required to adjust the pH from 7.0 to 8.7 for 1 $m^3$ wastewater, and the corresponding cost was 0.12 kg×2.5 CNY $kg^{-1}$ = 0.3 CNY. After optimization, although the acid-base adjustment cost was slightly increased, combined with the significant reduction in catalyst cost, the integrated raw material

cost still achieved a net saving of 71.7 CNY for treating 1 $m^3$ wastewater, with a reduction of 17.7 %.

*2) Comparative analysis of operation cost*. Table S-V of the Supplementary material gives the comparative analysis of operation cost before and after optimization. The energy consumption of photocatalytic reaction mainly came from the xenon lamp (300 W) and the stirrer (50 W). The energy consumption was positively correlated with the reaction time. Before optimization, the energy consumption for treating 1 $m^3$ wastewater was (300 W + 50 W)×3 h = 1.05 kWh and the corresponding energy cost was 1.05 kWh×0.6 CNY $kWh^{-1}$ = 0.63 CNY. After optimization, the reaction time was 127 min (2.12 h). Therefore, the energy consumption for treating 1 $m^3$ wastewater was (300 W + 50 W)×2.12 h = 0.742 kWh, and the corresponding energy cost was 0.742 kWh×0.6 CNY $kWh^{-1}$ = 0.445 CNY. Therefore, after optimization, the energy consumption cost for treating 1 $m^3$ wastewater was reduced by 0.185 CNY, with a decrease of 29.4 %.

With regard to the labor cost, before optimization, assuming that the operation time of a single batch treatment of 1 $m^3$ wastewater was about 3.5 h, the labor cost was 3.5 h×30 CNY $h^{-1}$ = 105 CNY. After optimization, the operation time was shortened to 2.5 h, and the labor cost was 2.5 h×30 CNY $h^{-1}$ = 75 CNY. Therefore, the labor cost for treating 1 $m^3$ wastewater was directly reduced by 30 CNY, with a decrease of 28.6 %.

*3) Comparative analysis of integrated cost*. Based on the raw material and operation costs, the integrated cost for treating 1 $m^3$ MB wastewater was calculated. Before optimization, the integrated cost for treating 1 $m^3$ MB wastewater was (400 + 0 + 0.63 + 105) CNY= 505.63 CNY. After optimization, the integrated cost for treating 1 $m^3$ MB wastewater was (328 + 0.3 + 0.445 + 75) CNY = 403.745 CNY. Therefore, after optimization, the integrated cost for treating 1 $m^3$ MB wastewater was reduced by 101.885 CNY, with a decrease of 20.0 %.

## CONCLUSION

In this work, S-doped g-$C_3N_4$ was successfully prepared by a facile one-step pyrolysis approach, using thiourea as the precursor and sulfur source. The as-prepared sample was characterized by XRD, FTIR, FESEM, TEM, EDS and UV–Vis DRS. The sample exhibited a wide visible-light absorption region, and its $E_g$ was estimated to be 2.63 eV. Furthermore, an additional absorption feature near 645 nm was observed in the UV–Vis DRS spectrum, corresponding to an $E_g$ of 1.81 eV. This might be associated with an S-induced impurity energy level in the band structure. The as-prepared sample exhibited stronger photocatalytic performance toward MB degradation. After 120 min of photocatalytic irradiation, the MB degradation rate reached 95.8 %. Based on RSM under CCD, the process optimization of MB photodegradation over the S-doped g-$C_3N_4$ photocatalyst was

conducted. Based on the economic cost calculations, after optimization, the integrated cost for the photodegradation of 1 $m^3$ MB wastewater over S-doped g-$C_3N_4$ was reduced from 505.63 to 403.745 CNY, with a decrease of 20.0 %.

## SUPPLEMENTARY MATERIAL

Additional data and information are available electronically at the pages of journal website: https://www.shd-pub.org.rs/index.php/JSCS/article/view/13775, or from the corresponding author on request.

ИЗВОД

## ОПТИМИЗАЦИЈА ПРОЦЕСА И ЕКОНОМСКИ ПРОРАЧУН ФОТОКАТАЛИТИЧКЕ ДЕГРАДАЦИЈЕ МЕТИЛЕНСКОГ ПЛАВОГ КОРИШЋЕЊЕМ g-$C_3N_4$ ДОПИРАНОГ СУМПОРОМ

WEI LI[1] и SHUYU CAO[2]

*[1]Department of Economics, Heilongjiang University of Finance and Economics, Harbin 150025, China и [2]Department of Science and Technology, Heilongjiang University of Finance and Economics, Harbin 150025, China*

Допирање сумпором сматра се ефикасном стратегијом за побољшање фотокаталитичке активности графитног нитрида угљеника (g-$C_3N_4$). Међутим, у литератури нису присутни извештаји о оптимизацији овог процеса, као ни о економском прорачуну при одређивању оптималних фотокаталитичких параметара. У овом раду, g-$C_3N_4$ допиран сумпором (S/g-$C_3N_4$) припремљен је *in situ* методом пиролизе у једном кораку, уз коришћење тиоурее као прекурсора и извора сумпора. У раду је извршена карактеризација S/g-$C_3N_4$ различитим инструменталним техникама. За одређивање оптималних фотокаталитичких услова за деградацију метиленског плавог (MB) коришћењем S/g-$C_3N_4$ коришћена је метода одзивне површине (RSM). Успостављен је дизајн експеримента са четири фактора на пет нивоа, који је обухватио 30 експерименталних понављања. Добијени су следећи оптимални услови: почетна концентрација MB од 27,6 mg $L^{-1}$, доза катализатора 4,1 g $L^{-1}$, pH раствора 8,7 и време реакције 125 min. Под овим условима, предвиђена ефикасност деградације достиже 99,94 %, док је експериментална вредност износила 99,5 %. Анализа трошкова показала је да оптимизација значајно смањује директне трошкове, у великој мери побољшава искоришћеност опреме и повећава оперативну флексибилност. Овај рад поставља кључну основу за контролу трошкова и повећање ефикасности при примени фотокатализатора на бази g-$C_3N_4$ у индустријским размерама.

(Примљено 12. фебруара, ревидирано 10. априла, прихваћено 19. маја 2026)

## REFERENCES

1. X. Z. Tang, Y. M. Xin, R. H. Chen, X. F. Ren, L. G. Gao, H. Xu, P. X. Yang, A. M. Liu, *J. Mater. Chem., A* **13** (2025) 34122-34148 (https://doi.org/10.1039/d5ta04748j)
2. G. Kavitha, M. Govindhan, S. Premkumar, *J. Water Process Eng.* **80** (2025) 109071 (https://doi.org/10.1016/j.jwpe.2025.109071)
3. M. S. N. Awang, B. L. Phoon, W. M. A. W. Daud, S. Boonyuen, J. C. Juan, *Mater. Sci. Eng., B* **324** (2026) 119025 (https://doi.org/10.1016/j.mseb.2025.119025)
4. X. S. Wang, Z. Y. Yuan, *Coord. Chem. Rev.* **548** (2026) 217184 (https://doi.org/10.1016/j.ccr.2025.217184)

5. M. Q. Xiao, J. J. Kong, W. J. Wang, B. Yang, S. Q. Guo, *J. Alloys Compd.* **1046** (2025) 184670 (https://doi.org/10.1016/j.jallcom.2025.184670)
6. J. Avinash, G. Madhumitha, S. M. Roopan, *J. Environ. Chem. Eng.* **13** (2025) 118368 (https://doi.org/10.1016/j.jece.2025.118368)
7. M. W. Xu, Y. J. Wu, X. Z. Zhao, J. Wang, G. C. Jiang, S. Li, Z. Q. Li, *J. Alloys Compd.* **1042** (2025) 184188 (https://doi.org/10.1016/j.jallcom.2025.184188)
8. M. G. Sahini, A. Parmain, I. Onoka, S. F. Mwanga, *J. Alloys Compd.* **1044** (2025) 183642 (https://doi.org/10.1016/j.jallcom.2025.183642)
9. N. Farooq, N. Qureshi, S. Hussain, A. M. Qureshi, Z. Sattar, R. K. Manavalan, N. Ullah, M. K. Aslam, *Int. J. Hydrogen Energy* **180** (2025) 151763 (https://doi.org/10.1016/j.ijhydene.2025.151763)
10. H. Noreen, A. Farooq, S. Naz, N. Amjed, A. Ahmad, A. Aftab, S. Muzammal, *J. Iran. Chem. Soc.* **22** (2025) 1659 (https://doi.org/10.1007/s13738-025-03252-6)
11. M. Zheng, M. R. Guo, F. Ma, W. W. Li, Y. J. Shao, *Nanoscale Adv.* **7** (2025) 4780 (https://doi.org/10.1039/d5na00439j)
12. C. Wen, Z. W. Xie, X. X. Gao, L. Q. Feng, Z. H. Li, P. C. Li, A. L. Wang, J. Wang, W. Q. Yao, *Colloids Surfaces, A* **727** (2025) 138402 (https://doi.org/10.1016/j.colsurfa.2025.138402)
13. H. L. Xu, X. F. Peng, J. X. Zheng, Z. Wang, *Front. Chem. Sci. Eng.* **17** (2023) 93 (https://doi.org/10.1007/s11705-022-2175-x)
14. L. Ma, S. Z. Hu, P. Li, Q. Wang, H. F. Ma, W. Li, *J. Phys. Chem. Solids* **118** (2018) 166 (https://doi.org/10.1016/j.jpcs.2018.03.017)
15. D. Yang, L. Zhao, X. T. Feng, L. L. Ma, H. M. Ding, *Funct. Mater. Lett.* **14** (2021) 2151019 (https://doi.org/10.1142/S179360472151019X)
16. W. L. Song, N. N. Zhang, X. J. Ma, X. T. Liu, D. N. Li, J. Li, *Chemistryselect* **9** (2024) e202400279 (https://doi.org/10.1002/slct.202400279)
17. M. X. Zuo, X. Y. Li, Y. S. Liang, F. X. Zhao, H. B. Sun, C. Liu, X. M. Gong, P. F. Qin, H. Wang, Z. B. Wu, L. Luo, *Sep. Purif. Technol.* **308** (2023) 122875 (https://doi.org/10.1016/j.seppur.2022.122875)
18. D. M. Azar, A. Feizbakhsh, H. A. Panahi, A. Niazi, *Int. J. Environ. Anal. Chem.* **102** (2022) 8490 (https://doi.org/10.1080/03067319.2020.1853114)
19. C. Y. Chen, Z. F. Luo, H. X. Tu, X. J. Lin, Y. W. Pang, J. F. Huang, J. Zhang, X. J. Wang, Q. Y. Cai, Z. B. Wei, J. Zeng, J. Qiu, *J. Hazard. Mater.* **486** (2025) 136986 (https://doi.org/10.1016/j.jhazmat.2024.136986)
20. H. M. Samuel, C. A. Mecha, M. M. M'Arimi, *React. Kin. Mech. Catal.* **137** (2024) 2415 (https://doi.org/10.1007/s11144-024-02650-w)
21. N. Szpisjak-Gulyás, A. N. Al-Tayawi, Z. H. Horváth, Z. Lászlo, S. Kertész, C. Hodúr, *Acta Aliment.* **52** (2023) 521 (https://doi.org/10.1556/066.2023.00235)
22. C. E. Aristizabal-Alzate, E. Castillejos-López, A. B. Dongil, M. Romero-Sáez, *Chemistryopen* **14** (2025) 202400148 (https://doi.org/10.1002/open.202400148)
23. H. Zhao, L. C. Wu, H. Y. Xu, *Sci. Adv. Mater.* **8** (2016) 1408 (https://doi.org/10.1166/sam.2016.2731)
24. M, Budych-Gorzna, L. Jaroszynski, P. Oleskowicz-Popiel, *J. Environ. Chem. Eng.* **9** (2021) 106366 (https://doi.org/10.1016/j.jece.2021.106366)
25. M. Yao, Z. Ju, Z. Ran, T. Chen, H. Pan, *J. Water Process Eng.* **69** (2025) 106626 (https://doi.org/10.1016/j.jwpe.2024.106626)
26. K. Wu, S. Y. Li, F. Jiang, J. Wang, G. L. Liu, G. H. Chen, *Water Sci. Technol.* **68** (2013) 530-536 (https://doi.org/10.2166/wst.2013.247)

27. J. Yang, X. Zhang, C. Xie, Ji. Long, Y. Wang, L. Wei, X. Yang, *J. Electron. Mater.* **50** (2021) 1067 (https://doi.org/10.1007/s11664-020-08654-1)
28. Q. H. Shen, C. Y. Wu, Z. Y. You, F. L. Huang, J. S. Sheng, F. Zhang, D. Cheng, H. Yang, *J. Mater. Res.* **35** (2020) 2148 (https://doi.org/10.1557/jmr.2020.182)
29. G. Nabi, N. Malik, W. Raza, *Inorg. Chem. Commun.* **119** (2020) 108050 (https://doi.org/10.1016/j.inoche.2020.108050)
30. S. Challagulla, S. Payra, C. Chakraborty, S. Roy, *Phys. Chem. Chem. Phys.* **21** (2019) 3174 (https://doi.org/10.1039/C8CP06855K)
31. Y. C. Ren, T. Gong, S. L. Tan, M. Chen, F. Zhou, Y. Lin, L. Yang, Q. Peng, *J. Alloys Compd.* **902** (2022) 163752 (https://doi.org/10.1016/j.jallcom.2022.163752)
32. L. F. Wang, Z. Y. Fan, X. X. Cao, P. F. Fan, Y. Xie, Q. Sun, J. S. Zhao, *Nanomaterials* **12** (2022) 2569 (https://doi.org/10.3390/nano12152569)
33. A. M. Li, X. H. Cong, H. T. Qin, W. C. Xu, X. H. Zhang, W. Z. Wang, F. Guo, *New J. Chem.* **47** (2023) 3910 (https://doi.org/10.1039/D2NJ06154F)
34. L. Dong, H. W. Chu, S. P. Xu, Y. Li, S. Z. Zhao, D. C. Li, *Nanophotonics* **11** (2022) 139 (https://doi.org/10.1515/nanoph-2021-0549)
35. B. Hernández, C.G. Blázquez, V. Aristizábal-Marulanda, M. Martín, *Ind. Eng. Chem. Res.* **59** (2020) 16720 (https://doi.org/10.1021/acs.iecr.0c03336)
36. D. H. Zhang, J. W. Liu, H. Wang, Y. Y. Wang, *Environ. Res.* **290** (2026) 123449 (https://doi.org/10.1016/j.envres.2025.123449)
37. K.-J. Wang, P.-S. Wang, *J. Water Process Eng.* **78** (2025) 108703 (https://doi.org/10.1016/j.jwpe.2025.108703).